Use of salt caverns in the energy transition: Application to Power-to-Gas–Oxyfuel

Laura Blanco Martín, Ahmed Rouabhi, Faouzi Hadj-Hassen

Use of salt caverns in the energy transition: application to Power-to-Gas–Oxyfuel

Laura Blanco-Martín[a,*], Ahmed Rouabhi[a], Faouzi Hadj-Hassen[a]

[a] *MINES ParisTech, Department of Geosciences, PSL Research University, 35 rue Saint Honoré, 77300 Fontainebleau, France*

Abstract

Power-to-Gas–Oxyfuel, or Electrolysis-Methanation-Oxyfuel, is an advanced concept that addresses some concerns of conventional Power-to-Gas: supply of high-purity CO_2, release of greenhouse gases to the atmosphere and fate of the O_2 from electrolysis. Due to the intermittent nature of several renewable energy sources, massive storage is needed to balance supply and demand. This paper focuses on the storage phase required for Electrolysis-Methanation-Oxyfuel. Synthetic CH_4, O_2 and CO_2 have to be stored at different times. Due to the high fluid rates and volumes required, salt caverns are potential candidates. While salt caverns have been used for decades to store CH_4, storage of CO_2 and O_2 has not been implemented to date. A generic seasonal scenario with a 200 MW oxyfuel unit is investigated. Numerical modeling that couples cavern thermodynamics with the thermo-mechanical response of the surrounding rock salt has been performed. The results, although exploratory, show that the caverns would be stable as they respect the criteria commonly used for cavern design. Moreover, combined storage of CO_2 and O_2 in the same cavern, rather than independent stor-

*Corresponding author
Email address: laura.blanco_martin@mines-paristech.fr (Laura Blanco-Martín)

age, would reduce the number of caverns needed and the likelihood of phase changes, but it would require separation of the two substances at the ground surface.
Key words: Underground energy storage, Salt caverns, Thermomechanical modeling, Thermodynamics, Power-to-Gas–Oxyfuel

1. Introduction

The energy transition from fossil to low-carbon energy requires an increasing share of renewable energy sources in the energy mix. For instance, the French roadmap targets 30% of renewable energy in the global energy mix by 2030 and a 75% reduction in greenhouse gas emissions below 1990 levels by 2050 [1]. Due to the intermittent nature of renewable sources of energy such as solar and wind, massive energy storage is necessary to succeed in the energy transition. In recent years, Power-to-Gas (PtG) has emerged as a promising option for handling high shares of renewable energy [2, 3] because it provides large-scale, long-term flexible energy storage [4, 5]. In this technology, excess renewable electrical power is used to produce H_2 and O_2 *via* water electrolysis. In this way, electricity, which cannot be currently stored in considerable quantities, is converted into gas; the produced H_2 can be stored/used directly (industry, transportation, power generation, injection into the gas grid, etc.), or it can be combined with a suitable source of CO_2 to produce synthetic natural gas (SNG) *via* methanation. There are currently PtG pilot plants in several countries such as Germany, Switzerland, USA, Canada, France, Denmark and Japan [4, 6–9]. The main reactions involved in PtG are

$$H_2O \rightarrow H_2 + {}^1/_2O_2 \tag{1}$$

for water electrolysis and the Sabatier reaction for methanation [10, 11]. This reaction, combined with consecutive inverse water-gas shift and CO methanation, leads to the production of SNG:

$$\begin{aligned} CO_2 + 4H_2 &\leftrightarrows CH_4 + 2H_2O \\ CO_2 + H_2 &\leftrightarrows CO + H_2O \\ CO + 3H_2 &\leftrightarrows CH_4 + H_2O \end{aligned} \tag{2}$$

Some drawbacks of PtG include cost-effectiveness (although costs are decreasing [8]), the availability of a suitable CO_2 (or CO) source for methanation, and the current lack of valorisation of the oxygen produced during electrolysis. To address these drawbacks, hybrid PtG systems have been proposed [12–14].

This work investigates the combination of PtG with oxyfuel combustion, which leads to Electrolysis-Methanation-Oxyfuel (EMO), a process comprising an energy storage phase (PtG) and an energy withdrawal phase (Gas-to-Power, GtP, through oxyfuel combustion of the stored SNG). In this process, the O_2 from electrolysis (rather than air) is used as the oxidizing agent in the GtP step; in this way, not only is the O_2 valorised, but the flue gases from the GtP step are also theoretically free of NO_x, as they only comprise CO_2 and steam (see Eq. (3)). Moreover, the CO_2 produced during the combustion of SNG is quite pure and can be used to feed the methanation process; in fact, Eqs. (1-3) show that EMO can function in a closed loop for the supply of the needed reactants in the generation of fluid carriers [15]. Fig. 1 shows a schematic diagram of EMO, including the unit

systems and the flow of the fluids.

$$CH_4 + 2O_2 \leftrightarrows CO_2 + 2H_2O \tag{3}$$

Several aspects of EMO have been studied in recent years, such as steady-

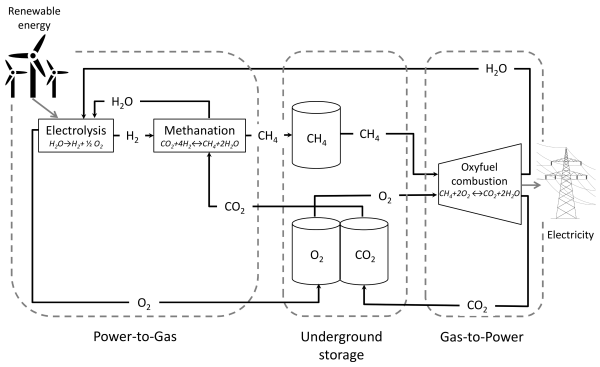

Figure 1: Schematic representation of EMO (Electrolysis-Methanation-Oxyfuel). The arrows indicate the circulation of the fluids according to the chemical reactions

state and dynamic behaviour of the unit processes, utilization of waste heat and overall efficiency [15–17]. From an economic point of view, a recent study has shown that EMO is currently only competitive for seasonal storage [18]; for short-term storage (weeks, days or even less), other technologies such as CAES or pumped storage (PSPS) are more competitive. In this study, the focus is on the storage phase of EMO, which is poorly documented in the literature: during the PtG phase, O_2 and CH_4 are generated and must be stored for subsequent combustion, and CO_2 is withdrawn from storage. In turn, during the GtP phase, O_2 and CH_4 are withdrawn from storage and the produced CO_2 is stored until the next PtG phase. Thus, CH_4, O_2 and CO_2 have to be stored at different times. Storage of CH_4 in salt caverns has occurred since the 1960s [19, 20] and is a well-known technology [21];

however, CO_2 and O_2 have not yet been stored in salt caverns, despite some research being conducted for the former [22, 23], including a recent study related to PtG [24]. Since massive quantities of these products are required for EMO, underground storage is the most convenient option [25, 26]. Additionally, flexible, high fluid rates will be required. As salt caverns satisfy the requirements for both large volumes and high fluid rates [27] (in addition to low cushion requirements and low investment & operation costs, as well as very low porosity and near-zero permeability of the host rock in the undisturbed state), they are a promising choice [28].

This paper investigates storage of CH_4, O_2 and CO_2 in salt caverns within the framework of EMO. While CH_4 is stored independently, two configurations are studied for the new substances, CO_2 and O_2: independent storage in separate caverns and storage as a mixture in the same cavern. First, the thermodynamic behaviour of the different products is assessed in the relevant conditions for underground storage. Available data for CO_2-O_2 mixtures (less documented than the pure substances) are used to validate the predictions of a recent high-accuracy equation-of-state (EOS) [29]. The governing equations of the thermodynamic problem in the cavern are briefly presented. The thermomechanical behaviour of rock salt and the governing equations of the thermomechanical problem are shortly described, as well as common criteria used to evaluate cavern stability: evolution of cavern pressure [30, 31], volume loss rate [32, 33], no tensile stresses [34, 35], and no dilatancy [36, 37]. Then, a generic scenario, *i.e.,* not site-specific, consisting of seasonal storage for the generation of 200 MW of electric power is presented. The depth of the caverns center is assumed to be 1200 m. Caverns stability is investigated for the different products and configurations (independent *vs.* combined storage for CO_2 and O_2). Although the results

presented are exploratory, they suggest that the caverns would be stable and that storing a mixture of CO_2 and O_2 would have three main advantages: the risk of phase changes decreases compared to that of pure CO_2, compressibility increases, and the fluids replace each other in the storage phase, leading to a reduction in the number of caverns needed. However, separation of the two substances would be necessary at the ground surface, which could be achieved using membranes [38]. This work illustrates a methodology that combines cavern thermodynamics with the thermomechanical long-term response of rock salt, and identifies future research paths to advance the maturity of EMO, as well as the use of salt caverns in the energy transition context.

2. Materials and Methods

2.1. Thermodynamics of the stored products and cavern governing equations

The critical pressure and temperature of CH_4 are $P_c = 4.6$ MPa and $T_c = 190.6$ K, respectively [39]; therefore, in a typical seasonal storage, CH_4 is in supercritical or gaseous conditions. The same would apply to O_2 storage in salt caverns since its critical pressure and temperature are 5.0 MPa and 154.6 K, respectively [40]. For CO_2, $P_c = 7.4$ MPa and $T_c = 304.1$ K [41]; in this case, phase changes are likely to occur depending on the cavern depth, injection & withdrawal rates, cycling frequency and injection conditions. Phase changes during salt cavern operation would complicate standard use and should be avoided whenever possible; indeed, a literature review suggests that storage in salt caverns occurs under single-phase conditions, and therefore additional investigations are necessary prior to considering phase changes. When the stored fluid has a low compressibil-

ity (such as in the case of liquids), brine compensation is used (*i.e.*, during fluid withdrawal/injection, brine is injected/withdrawn through the central tubing to withdraw/inject an equivalent volume of fluid through the annular space [note that this requires a brine pond at the ground surface]), and the cavern pressure is approximately constant [42]. When the stored fluid is compressible (such as in the case of gases), pressure builds up during injection and decreases during withdrawal (brine is not required); in this case, the cavern pressure typically varies between 20% and 80% of the *in situ* initial stress both to minimize the amount of cushion gas and to ensure cavern stability [43–45]. If a phase change occurred, the operation method would need to be reviewed. For instance, if the product is initially in the gaseous state and the pressure increases sufficiently, it may become liquid, with low compressibility; further cavern exploitation would require a switch to the brine compensation technique, which would be difficult to put in place at the surface installations (brine availability, well architecture, etc.). A second feature of CO_2 is that it is more soluble in brine than either CH_4 or O_2 [46–48]; therefore, it would be more appropriate to avoid brine compensation methods to minimize mass transfer between CO_2 and brine.

Within the context of EMO, combined storage of CO_2 and O_2 is contemplated. Storing a mixture would be beneficial from three viewpoints: (i) as the amount of O_2 increases, the two-phase domain shifts towards lower temperatures and higher pressures, reducing the likelihood of phase changes in the $P-T$ conditions of a typical storage (see Fig. 2), (ii) the compressibility of the mixture increases compared to that of pure CO_2, and (iii) since CO_2 and O_2 are injected/withdrawn at different steps of the process, they replace each other in the storage phase, thereby reducing the number of caverns needed for a given working mass. The main disadvantage

of storing a mixture is that a separation technique would be required at the ground surface, such as membrane separation, liquid absorption, or adsorption [49]. The applicability of these techniques to CO_2-O_2 mixtures exceeds the scope of the current work and must be further investigated. Indeed, a literature review shows that most research has been performed in the contexts of oxy-combustion and carbon capture and storage (CCS), and does not focus on CO_2-O_2 separation [50–53]. Membrane separation is an energy-efficient, inexpensive approach compared to other options, and it results in low environmental impacts [54]. Given the thermodynamic conditions characteristic of EMO and the different molecular sizes of CO_2 and O_2, membrane separation is a promising technique, with CO_2 recovery rates of up to 90%, obtained purity greater than 95 mol% and energy consumption between 0.25 and 0.38 kWh/kg of separated CO_2 [54].

In this work, the thermodynamic behaviour of the different stored products is described using high-accuracy EOS explicit in the Helmholtz free energy, whose canonical variables are temperature, T, density, ρ and molar composition, $\vec{c}$ [55]. Written in dimensionless form, such EOS reads

$$f(\rho, T, \vec{c}) = f^0(\rho, T, \vec{c}) + f^r(\delta, \tau, \vec{c}) \tag{4}$$

with

$$f^0(\rho, T, \vec{c}) = \sum_{i=1}^{n} c_i[\ln c_i + f_i^0(\rho, T)] \tag{5}$$

and

$$f^r(\delta, \tau, \vec{c}) = \sum_{i=1}^{n} c_i f_i^r(\delta, \tau) + \Delta f^r(\delta, \tau, \vec{c}) \tag{6}$$

where $n \geq 1$ is the number of components, $\delta = \rho/\rho_r(\vec{c})$ is the reduced density, $\tau = T_r(\vec{c})/T$ is the inverse reduced temperature, and $\rho_r(\vec{c})$ and $T_r(\vec{c})$

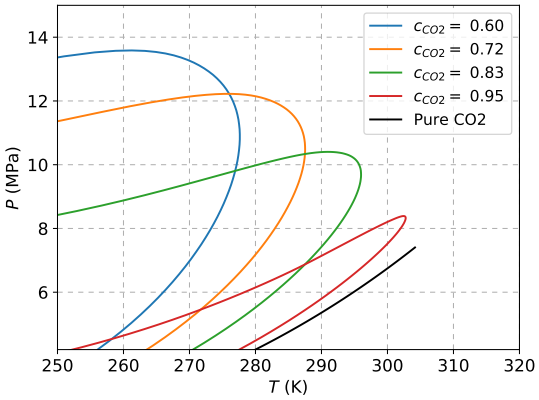

Figure 2: P-T envelope of the CO_2-O_2 mixture for different molar fractions and $T \geq 250$ K [29]. For each composition shown, the inner region corresponds to the two-phase domain

are the composition-dependent reducing functions [55]. In Eqs. (4-6), f^0 represents the ideal gas mixture behaviour and f^r represents the residual mixture behaviour. The main advantage of such EOS is that all thermodynamic properties of a mixture or pure substance can be obtained by properly combining derivatives of Eqs. (4-6); these properties will be needed to solve for the thermodynamic state of the cavern in the system of equations (7).

For the CO_2-O_2 mixture, which is less documented than the pure substances, coefficients for Eq. (6) as well as for $\rho_r(\vec{c})$ and $T_r(\vec{c})$ have been recently published ([29] and references therein). As seen in Fig. 3, the comparison between available experimental data and EOS predictions is quite satisfactory (the comparison is limited to single-phase $P\rho T$ data because published data on the two-phase domain or on caloric properties could not be found). New $P\rho T$ data for additional mixture compositions have been recently pub-

lished [56]. Additional investigations, including CO_2-O_2 phase changes, are necessary to fully characterize this mixture.

The governing equations of the thermodynamic problem in the cavern are

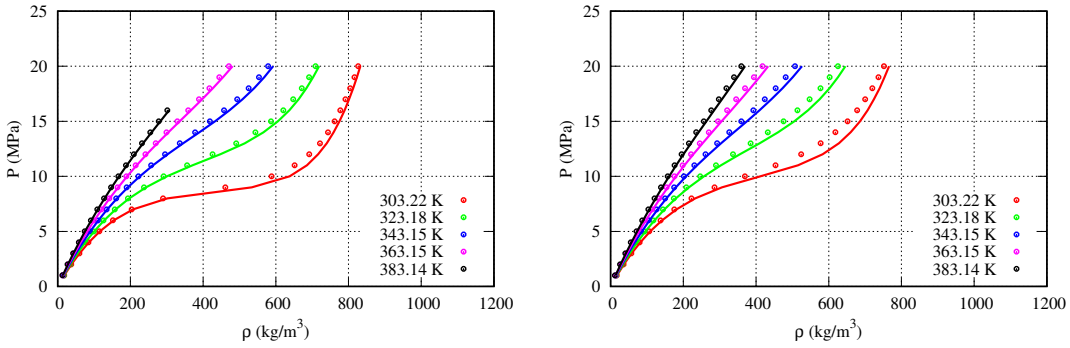

Figure 3: $P\rho T$ data of the CO_2-O_2 mixture for two molar fractions: (a) c_{CO_2}=0.939, (b) c_{CO_2}=0.871. Symbols correspond to experimental data [57] and lines correspond to predictions using Eqs. (4-6)

mass and energy balances. The approach described in [58] is used. Pressure and temperature are assumed to be uniform within the cavern, and their temporal evolution can be expressed as

$$\begin{pmatrix} A_{11} & A_{12} \\ A_{21} & -TA_{11} \end{pmatrix} \begin{pmatrix} \dot{T} \\ \dot{P} \end{pmatrix} = \begin{pmatrix} \dot{\mathcal{W}} \\ \dot{\Psi} \end{pmatrix} \tag{7}$$

where $\dot{\mathcal{W}}$ is the current cavern volume variation, adjusted by the variations in the partial volumes of the different species. The term $\dot{\Psi} = \dot{\Psi}_\sigma + \dot{\Psi}_I$ is the sum of the heat exchanged with the surrounding rock salt and the heat resulting from the fluid mass entering the cavern. Coefficients A_{11}, A_{12} and A_{21} depend upon the updated cavern volume and, respectively, upon the

isobaric thermal expansion coefficient, the isothermal compressibility factor and the isobaric specific heat capacity of each separate phase present in the cavern (stored fluid, brine).

2.2. Thermomechanical behaviour of rock salt, governing equations and stability criteria

Rock salt exhibits time-dependent behaviour and has interesting mechanical and flow properties for use as a disposal or storage medium, such as very low porosity, near-zero permeability in the undisturbed state, ductility, high thermal conductivity and healing capacity ([59] and references therein). For these reasons, rock salt has been extensively studied. Here, the approach described in [58] is used, in which rock salt is assumed to be a homogeneous, infinite elasto-viscoplastic medium with uniform initial temperature and uniform isotropic initial stress; these values are the averages over the cavern surface of the geothermal temperature and the geostatic stress, respectively. Likewise, the cavern pressure is averaged over the cavern surface. Hydraulic effects are neglected in the current exploratory study: according to laboratory and field measurements, rock salt permeability and porosity are very small in the undisturbed state, *e.g.* [60–68], and the accurate determination of the required parameters, such as Biot and Skempton coefficients or the gas entry pressure, is still an open question requiring difficult tests [69]. In principle, if the dilatancy domain is not reached, flow properties are not altered [45]. A review of salt caverns worldwide suggests that microfractures may open in a thin zone at the cavern wall, without compromising the barrier integrity of the salt rock mass [70]. Additionally, feedback from the salt cavern industry over the past 60 years suggests that thermomechanical effects within the rock salt prevail over hydraulic effects;

in fact, the access well is more prone to tightness loss (quality of the cementation, years of operation, geological anomalies, etc.) than the cavern itself [70, 71]. Note that cavern abandonment requires the study of hydraulic effects [45, 70, 72], but it is out of the scope of the current work, which focuses on the operation phase.

The governing equations of the thermomechanical problem within the rock are momentum and energy balances, which read, respectively,

$$\begin{aligned} \vec{\nabla} \cdot \underline{\underline{\sigma}} + \rho \vec{g} &= \vec{0} \\ \rho C_\sigma \dot{T} + \vec{\nabla} \cdot \vec{\psi} &= 0 \end{aligned} \tag{8}$$

where $\underline{\underline{\sigma}}$ is the Cauchy stress tensor, $\vec{g}$ is the gravity acceleration vector, ρ is the mass density, C_σ is the specific heat capacity at constant stress, $\dot{T}$ is the material derivative of the temperature T, $\vec{\psi}$ is the heat flux vector and $\vec{\nabla}\cdot$ is the divergence operator. The system (8) has to be completed with initial conditions, boundary conditions and constitutive laws for $\underline{\underline{\sigma}}$ and $\vec{\psi}$. Boundary conditions at the cavern wall are provided by the thermodynamic state of the cavern, described in the previous section. Eqs. (7-8) are solved iteratively within a time step using an in-house code, Demether [58]. Regarding the constitutive laws, for the heat flux Fourier's law is used, $\vec{\psi} = -\lambda \vec{\nabla} T$, where λ is the thermal conductivity of the rock. For the stress tensor, a constitutive law based on the additive decomposition of the strain rate tensor into elastic, thermal and viscoplastic components is used. Under the assumptions of infinitesimal elastic strains, isotropic material behaviour and negative signs for compressive stresses and strains, this yields

$$\underline{\underline{D}} = \frac{1+\nu}{E} \dot{\underline{\underline{\sigma}}} - \frac{\nu}{E} tr\left(\dot{\underline{\underline{\sigma}}}\right) \underline{\underline{1}} + \alpha_{th} \dot{T} \underline{\underline{1}} + \underline{\underline{D}}^{vp} \tag{9}$$

where $\underline{\underline{D}}$ is the Eulerian strain rate tensor, ν is the Poisson's ratio, E is the Young's modulus, α_{th} is the linear thermal expansion coefficient, $tr()$ is the

trace operator, $\underline{\underline{1}}$ is the identity tensor, and $\underline{\underline{D}}^{vp}$ is the viscoplastic strain rate tensor, which describes the time-dependent behaviour of rock salt. In this study, the evolution law of $\underline{\underline{D}}^{vp}$ is modeled using the Lemaitre creep law [58, 73], which can be expressed as

$$\underline{\underline{D}}^{vp} = \frac{3}{2}\frac{\dot{\gamma}}{q}\underline{\underline{\sigma}}^{'} \tag{10}$$

where $\underline{\underline{\sigma}}^{'} = \underline{\underline{\sigma}} - \frac{1}{3}tr\left(\underline{\underline{\sigma}}\right)\underline{\underline{1}}$ is the deviatoric stress tensor, $q = \sqrt{3/2}||\underline{\underline{\sigma}}^{'}||$ is the von Mises equivalent stress, and γ is an internal scalar variable whose evolution law accounts for material hardening and reads

$$\frac{d\gamma^{1/\alpha}}{dt} = \left(\frac{q}{K(T)}\right)^{\beta/\alpha}, K(T) = K_r \exp\left(B\left(\frac{1}{T} - \frac{1}{T_r}\right)\right) \tag{11}$$

where $(\alpha, \beta, K_r, B) \in \mathbb{R}_+^{*4}$ are material constants and T_r is the absolute temperature at which K_r is determined.

From a stability viewpoint, several well-established criteria must be satisfied. As explained above, one of these criteria is that the cavern pressure should not vary beyond 20-80% of the *in situ* initial stress in order to limit the stress deviator (which enhances creep) and to prevent (micro)fracture creation and fluid infiltration through the cavern wall; this criterion is based on experience [74–76]. Moreover, since the tensile strength of rock salt is small, typically $< 1 - 2$ MPa, the stress state around the cavern should remain compressive over time. Dilatancy, or non-elastic volumetric strain increase, should also be avoided or limited, as it is related to microcracking and the possible creation of preferential flow paths, with an increase in porosity and permeability [77]. For the exploratory purposes of this work, the following linear dilatancy criterion is assumed, expressed in MPa [37]:

$$q = 1.3p + 2.5 \tag{12}$$

where $p = -\frac{1}{3} tr\left(\underline{\underline{\sigma}}\right)$ is the mean stress. This criterion is based on laboratory strain-controlled tests with mean stresses up to 28 MPa; this range covers the mean stresses in the scenario investigated in this work. Note, however, that for a more accurate assessment of dilatancy, a constitutive law including this phenomenon at the rheological level should be used instead. Another stability criterion is the cavern relative volume variation over time, as it reflects creep closure and the effect of cycling on the volume loss rate, and it is related to surface subsidence [33]. In practice, a rate of volume variation ≥ -1 %/year is considered acceptable [32].

3. Model Description

In the generic seasonal scenario considered, the depth of the caverns center is 1200 m. This depth is typical to store large fluid quantities [42, 78]. The admissible cavern operation pressure increases with depth [70], and since fluid density is an increasing function of pressure, the deeper the cavern the larger the fluid quantity that can be stored in a given volume (note however that a compromise needs to be found for each particular case [salt creep properties, cycling scenario, etc.], as the stress deviator, and therefore the cavern closure rate, also increase with depth). For each substance (CH_4, O_2, CO_2, CO_2-O_2), the cavern volume is optimized to minimize the proportion of cushion required while ensuring stability; as will be shown in the next section, this implies that the cavern radii vary between 26 and 32 m, assuming cylindrical caverns of height $h = 200$ m (typical height for the considered depth [65, 78]). For simplicity, we assume that each cavern is isolated, *i.e.,* it is not influenced by surrounding caverns. The sump, filled with saturated brine, represents 5% of the cavern volume. Mass transfer

between the stored fluid and brine is not taken into account, but brine is considered in the heat balance equation. The salt layer extends up to the ground surface, and the *in situ* initial stress and temperature at 1200 m are $\sigma_\infty = -25.9$ MPa and $T_\infty = 45$ °C , respectively. Laterally, the model extension is 1000 times the cavern radius to avoid boundary effects on the mechanical problem (the extent of the thermal influence is smaller). Properties of the rock salt are listed in Table 1. They are taken from the Mines ParisTech experimental database, and have been obtained by calibration of experimental results within the same salt facies (triaxial strain-controlled tests and creep tests) with the Lemaitre creep law described above. Their range of application is for temperatures up to 70 °C , mean stresses up to 30 MPa and stress deviators up to 60 MPa, which cover the scenario investigated. The initial stress field is isotropic and the geothermal gradient is 0.025 K/m.

Prior to the cycling phase, leaching and debrining are modeled to take into account the loading history and the stress evolution within the rock mass. During this phase, which lasts 3.5 years, the cavern pressure is approximately 14 MPa (halmostatic). Subsequently, forty 360-day cycles are modeled. The cavern temperature at the beginning of the cycling phase is T_∞ for all substances. As explained in the Introduction, EMO is currently only competitive for seasonal storage; in this context, and for the illustrative purposes of this generic study, we assume that the PtG and GtP phases last 6 months each, but other schedules are possible. The scenario investigated could correspond to an excess of renewable energy during the spring/summer and an increase in energy demand during the autumn/winter. During each cycle, the amount of each substance injected (withdrawn) during the PtG phase is withdrawn (injected) during the GtP phase; therefore, the mass is

Table 1: Rock salt properties used in the simulations

Thermo-physical parameters				
ρ (kg/m^3)	C_σ (J/kg/K)	λ (W/m/K)		
2200	800	5.8		
Thermo-elastic parameters				
α_{th} (K^{-1})	E (GPa)	ν (-)		
$4{\cdot}10^{-5}$	25	0.25		
Viscoplastic parameters (unit system is MPa, K, days, μm/m)				
α	β	K_r	B	T_r
0.3	3.24	0.72	771.6	303.15

constant over a cycle.

From an energetic point of view, the efficiency of the oxyfuel unit is $\eta_{oxy} = 58\%$ [15]. The produced power, 200 MW, is typical for a city with a population of around 300,000 [79]. The efficiency of the methanation unit is quite high, $\eta_{meth} = 84\%$ [15], due to the catalyzed reaction and the generation of power as a by-product by recovering heat from the reactors (methanation is highly exothermic). Electrolysis has an overall efficiency of $\eta_{elec} = 63\%$, which translates into a need for about 610 MW of renewable power. Polymer Electrolyte Membrane (PEM) electrolysis has been chosen in the current analysis since it is a promising technique for PtG plants due to its high performance under transient conditions. Further details about the energy performance of the system, including a sensitivity analysis of the different sub-systems, are given elsewhere [15, 17].

The methane mass rate used in our simulations is computed using Eq. (13),

and corresponds to the generation of $\mathcal{P} = 200$ MW in the oxyfuel unit with a CH_4 lower heating value (L_{HV}) of 50 MJ/kg, yielding 552960 kg/d ($\mathcal{P}_{aux}$ is the power consumption of auxiliaries, estimated to be about 15 MW [15]).

$$Q_{CH_4} = \frac{\mathcal{P} - \mathcal{P}_{aux}}{\eta_{oxy} L_{HV}} \tag{13}$$

The composition stoichiometry in the reactions (1-3) is used to compute the mass rates of the other substances, yielding $Q_{CO_2} = 1520640$ kg/d and $Q_{O_2} = 2211840$ kg/d; these rates are constant when CO_2 and O_2 are stored in separate caverns (note that the rates are positive during injection and negative during withdrawal). For the CO_2-O_2 mixture, the initial composition is $c_{CO_2} = 0.5$. During the PtG phase, pure O_2 from electrolysis is injected, and the mixture, rather than pure CO_2, is withdrawn for methanation; therefore, the composition in the cavern is not constant over time, as the net mass of O_2 increases and that of CO_2 decreases, and there is simultaneous injection and withdrawal, either through two different wells or through one well having two concentric spaces. Note that in this case, the rates of CO_2 and O_2 are not constant. It is assumed that the O_2 withdrawn jointly with the CO_2 is reinjected, so that the net mass variation of each substance is the same as in separate storage; in this way, it is possible to compare separate and combined storages. The opposite applies to the GtP phase. With the energy costs provided in section 2.1, the separation would require around 15 MW in the current scenario. In all cases, the substances are injected at 45 °C and 20 MPa ($\approx 80\%\ \sigma_\infty$). The withdrawal conditions (pressure, temperature, and eventually mixture composition) are determined internally by Demether, depending on the thermodynamic state of the product in the cavern. The themodynamic behaviour of the substances is modeled using Eqs. (4-6) with parameters from [39] for CH_4, from [55] for CO_2 and O_2, and

from [29] for the mixture. For each substance, the temperature and pressure ranges of application of the EOS cover the scenario investigated in this work.

4. Results and Discussion

The cavern pressure evolution during the cycling phase is shown in Fig. 4, and the temperature evolution is displayed in Fig. 5 (in the figures shown in this section, $t = 0$ is set to the beginning of the cycling phase). Note that the initial pressure is not the same for all substances; during PtG (initial phase), CH_4 and O_2 are injected, so the initial cavern pressure must be close to P_{min}. This is achieved by decreasing the cavern pressure after debrining and allowing thermal equilibrium with the surrounding rock. The initial temperature of the cycling phase is 45 °C in all cases.

As Fig. 4 shows, for CH_4 and O_2 the cavern pressure varies between

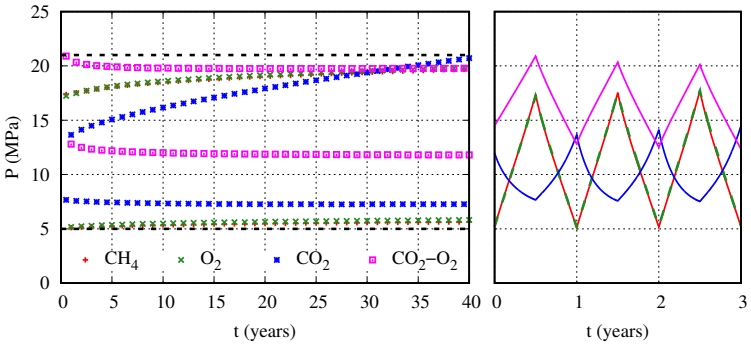

Figure 4: Pressure evolution for the different substances ($P_{max} = 20.7$ MPa and $P_{min} = 5$ MPa). On the left-hand side plot, for ease of interpretation only the values at the end of PtG and GtP are displayed, which correspond to the extreme values of each cycle. On the right-hand side plot, a detailed evolution during the first three cycles is displayed

$P_{min} = 0.2\ \sigma_\infty$ and $P_{max} = 0.8\ \sigma_\infty$, while for CO_2 the amplitude of the pressure variation is smaller in order to avoid phase changes ($P_c = 7.4$ MPa). CO_2 is in supercritical conditions, although not far from the critical point; in this region, its compressibility is low, which explains why the average P and T increase over time (for the other substances, maximum and minimum values of pressure stabilize by the end of the cycling phase), as well as the important proportion of cushion required, displayed in Table 2. However, this outcome is not considered a penalty since CO_2 is a greenhouse substance. In the case of the CO_2-O_2 mixture, the cavern pressure does not decrease below 12 MPa in order to prevent tensile stresses, as will be shown below. Note that the trends of cavern pressure are different for the different substances: for CH_4, O_2 and CO_2, the average pressure increases over time (more for CO_2, as explained above), whereas it decreases for the CO_2-O_2 mixture (this is due to the operation mode of the cavern, *i.e.*, simultaneous injection and withdrawal, with net injection during PtG and net withdrawal during GtP). These trends also apply to the temperature evolution in Fig. 5.

Fig. 4 shows that the cavern pressure remains within P_{max} and P_{min} for all substances. To achieve this goal, and given the high mass rates required to produce 200 MW of electric power (see Section 3), more than one cavern

Table 2: Mass percentage of cushion per cavern (values for CO_2-O_2 are not displayed because the cavern composition is not constant)

Substance	Cushion (%)
CH_4	29.2
O_2	32.7
CO_2	76.5

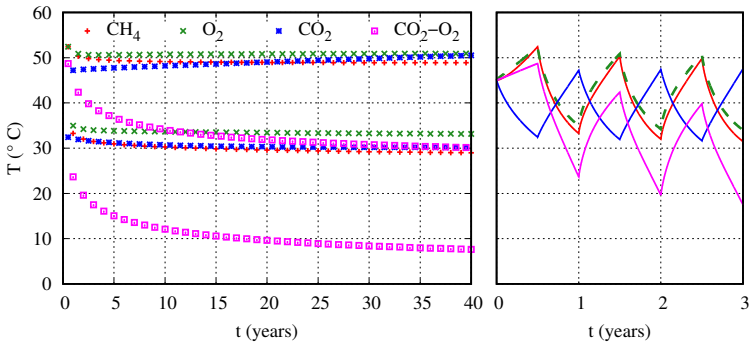

Figure 5: Temperature evolution for the different substances. On the left-hand side plot, for ease of interpretation only the values at the end of PtG and GtP are displayed, which correspond to the extreme values of each cycle. On the right-hand side plot, a detailed evolution during the first three cycles is displayed

is required per substance. The number and dimensions of the caverns are displayed in Table 3. These values, obtained numerically, correspond to the minimum number of caverns of the listed size that ensures cavern stability according to the criteria defined in Section 2.2. These dimensions are common for existing caverns at a similar depth [20, 42, 65, 78]. The differences are due to the different mass rates (related to the composition stoichiometry of the reactions (1-3)) and to the different thermodynamic behaviour of each substance. Note that 9 caverns would be needed if CO_2 and O_2 were stored independently, while 6 caverns would be required if they were stored in the same cavern. In the case of the mixture, the composition in the cavern varies between $c_{CO_2} = 0.5$ and $c_{CO_2} = 0.15$ during each cycle.

Fig. 5 shows that the temperature variation is approximately $\Delta T \approx 20$ °C for CH_4, O_2 and CO_2 and slightly larger for the mixture, particularly during the first cycles. The initial differences between CH_4, O_2 and

Table 3: Computed number of caverns and radius in the scenario studied ($h = 200$ m in all cases)

Substance	r (m)	Number of caverns
CH_4	26	3
O_2	28	6
CO_2	31	3
CO_2-O_2	32	6

CO_2 are partly due to the different regime (injection for the first two during PtG, and withdrawal for the latter [and the opposite during GtP]). Although all substances, including the mixture, cool upon expansion, their thermodynamic behaviour is not identical; this explains why ΔT is slightly smaller for O_2 than for CH_4, although their pressure evolution is very similar. In the case of the mixture, and similar to the pressure analysis, the temperature decreases over time because of the operation mode of the cavern.

The cavern relative volume variation is displayed in Fig. 6. The figure shows that most of the volume loss is due to the creep of the rock salt, while the influence of the cycles is less pronounced. However, the first withdrawal for CH_4, O_2 and CO_2 induces an important volume loss (approximately 4% for CO_2) due to the increase in the stress deviator, q. In each cycle, volume loss is greater than volume increase because q increases during withdrawal and decreases during injection (viscoplastic strains are dominant over elastic and thermal strains). Creep closure contributes to the pressure increase over time displayed in Fig. 4. The cavern closure evolution is very similar for CH_4 and O_2, which explains their similar pressure evolution given their high compressibility compared to that of the other substances. Regard-

ing the mixture, the relative volume variation is smaller than for the other substances because the stress deviator is smaller (in Fig. 4, the minimum cavern pressure for the mixture is approximately 12 MPa, higher than that for CH_4, O_2 and CO_2). Overall, after 40 years of operation, the maximum cavern volume loss is approximately 16%, which is an admissible amount as the corresponding rate, -0.4 %/year, is greater than -1%/year, and because the caverns are large (initial volume between 425000 and 600000 m^3).

The tangential (σ_θ) and vertical (σ_z) stresses at the cavern wall are dis-

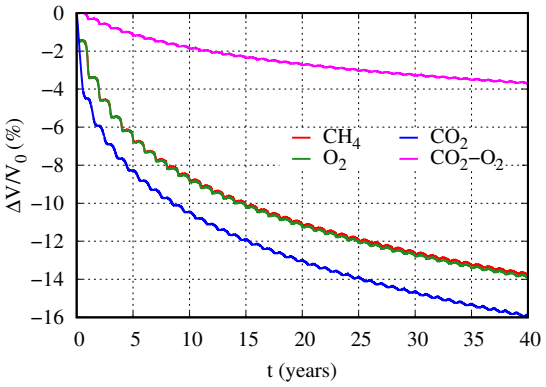

Figure 6: Cavern relative volume variation for the different substances

played in Fig. 7 for each substance. The stress state remains compressive over time, although it approaches 0 in the case of the CO_2-O_2 mixture; this is due to the larger thermal amplitude as shown in Fig. 5. The higher values of σ_z explain why the mixture requires the largest cavern volume and why the minimum cavern pressure is greater than P_{min} (see Fig. 4).

Finally, Fig. 8 shows the stress path in the $p - q$ plane, together with the dilatancy criterion defined in Eq. (12). As can be seen, the criterion is not reached for any substance. This criterion is often used for a first evaluation,

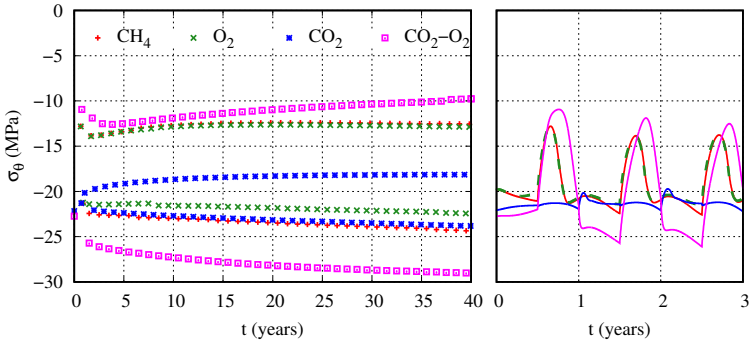

(a)

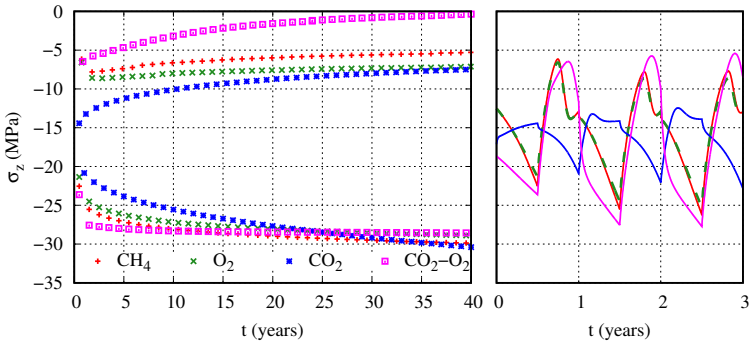

(b)

Figure 7: Evolution of (a) σ_θ and (b) σ_z for the different substances. On the left-hand side plot, for ease of interpretation only the extreme values of each cycle are displayed. On the right-hand side plot, a detailed evolution during the first three cycles is displayed

but in the case of a field application, an approach embedding dilatancy at the constitutive level should be used instead [37, 80].

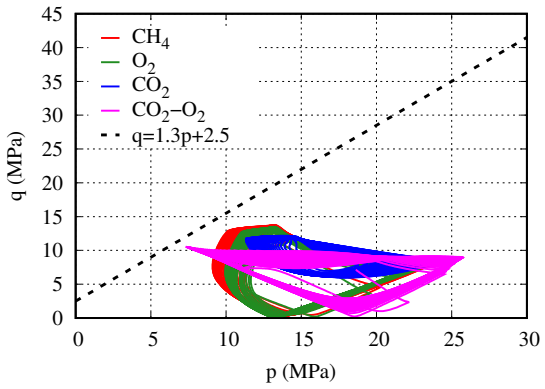

Figure 8: Stress path in the $p-q$ plane for the different substances

5. Conclusions and Perspectives

This paper focuses on the storage phase of Electrolysis-Methanation-Oxyfuel. Storage in salt caverns is investigated since it is a promising solution. A seasonal scenario is investigated because it is currently the only profitable possibility. Three substances, CH_4, O_2 and CO_2, have to be stored at different steps of the process: CH_4 and O_2 are stored during Power-to-Gas, and CO_2 is stored during Gas-to-Power. While CH_4 has been stored in salt caverns for decades, to the best of the authors' knowledge, there is no current storage of CO_2 or O_2 in salt caverns, which justifies the need for the current research.

The main goals of this work are to conduct a preliminary assessment of cavern stability and to investigate different storage configurations. For such purposes, we assume a uniform cavern response and perform simplified thermomechanical analysis of the rock salt, coupled with the thermodynamic behaviour of the stored substance. The studied scenario is generic and comprises 6 months of storage and 6 months of recovery to generate 200 MW

of electric power. Given that at present there is no site-specific data because EMO has not been implemented at the pilot or the industrial scales, we focus on the methodology (which combines the thermodynamic behavior of the stored fluids with the thermomechanical long-term response of rock salt), and illustrate it through a generic application.

The results obtained suggest that the salt caverns would be stable in the scenario studied since they respect common criteria for cavern design. The required mass rates of each substance are quite high, and to ensure cavern stability, 3 caverns would be required for CH_4, 6 caverns for O_2 and 3 caverns for CO_2, with volumes between 425000 and 600000 m^3. Regarding the storage configurations, storing a mixture of CO_2-O_2 presents three main advantages: the two-phase domain of CO_2 is shifted towards lower temperatures and higher pressures, the compressibility increases compared to that of pure CO_2, and the number of caverns required would be smaller (6 instead of 9) since simultaneous injection/withdrawal would be performed on the same cavern. The main disadvantage is that a separation technique would be necessary at the ground surface, such as membrane separation (in particular, ceramic membranes), liquid absorption or adsorption. For future site applications, an economic evaluation at the project scale considering all costs (permits, leaching infrastructure, brine disposal, wells, insurances, separation unit, etc.) should be conducted to decide on a storage configuration.

The results obtained in this theoretical work are exploratory but provide insight for further research, such as the acquisition of additional thermodynamic data for the CO_2-O_2 mixture ($P\rho T$ data for a wider range of mixture compositions, as well as caloric properties and study of the two-phase domain), or the investigation of the thermo(-hydro-)mechanical behaviour of

rock salt under storage conditions (creep under low and high stress deviators and under wide temperature ranges), as well as its coupling with the thermodynamic evolution of the stored fluid. In order to avoid extrapolations, the equations-of-state and geomechanical models used at the field scale should be based on experimental data that cover the range of interest. When available, field data should be used to check the predictions, perform recalibrations and improve the models.

Although Electrolysis-Methanation-Oxyfuel presents several advantages compared to conventional Power-to-Gas, its storage phase is quite complex, as three fluids need to be stored at different times in the process. Depending on the specificities of each real-scale case, it might be more profitable to perform electrolysis combined with a fuel cell, or to perform conventional methanation if a suitable source of CO_2 is available. For inter-seasonal storage, conventional methanation and fuel cells have levelized costs of storage similar to those of Electrolysis-Methanation-Oxyfuel. These three Power-to-Gas technologies are under development, and their relative competitiveness (technology costs, charge/discharge efficiency, etc.) may evolve in the future. It is also important to consider site selection aspects, such as availability of a salt formation with appropriate extension and properties (alternatively, leached caverns for brine production could be converted into storage caverns), proximity to renewable energy sources, eventually to CO_2 sources, to the grid, and to consumers.

Acknowledgments

Funding for this work has been partially provided by the French National Research Agency (ANR) under contract number 7747 (FluidSTORY project,

ID ANR-15-CE06-0015). The authors thank the partners of the project (Areva H_2Gen, Armines, BRGM, Brouard Consulting, Geogreen, Geostock and LMS-École Polytechnique) for the constructive discussions which have greatly improved the quality of the work presented.

References

[1] E. Combet, D. Marchal, I. Vincent, N. Mairet, V. Briand, Actualisation du scénario énergie-climat ADEME 2035-2050, Tech. Rep. 979-10-297-0921-0, ADEME (2017).

[2] M. Götz, J. Lefebvre, F. Mörs, A. McDaniel Koch, F. Graf, S. Bajohr, et al., Renewable Power-to-Gas: A technological and economic review, Renewable Energy 85 (2016) 1371 – 1390. doi:10.1016/j.renene.2015.07.066.

[3] M. Sterner, Bioenergy and renewable power methane in integrated 100% renewable energy systems. Limiting global warming by transforming energy systems, Ph.D. thesis, Kassel University (2010).

[4] M. Bailera, P. Lisbona, L. M. Romeo, S. Espatolero, Power to Gas projects review: Lab, pilot and demo plants for storing renewable energy and CO_2, Renewable and Sustainable Energy Reviews 69 (2017) 292 – 312. doi:10.1016/j.rser.2016.11.130.

[5] J. Vandewalle, K. Bruninx, W. D'haeseleer, Effects of large-scale power to gas conversion on the power, gas and carbon sectors and their interactions, Energy Conversion and Management 94 (2015) 28 – 39. doi:10.1016/j.enconman.2015.01.038.

[6] G. Gahleitner, Hydrogen from renewable electricity: An international review of Power-to-Gas pilot plants for stationary applications, International Journal of Hydrogen Energy 38 (5) (2013) 2039 – 2061. doi:10.1016/j.ijhydene.2012.12.010.

[7] K. Hashimoto, N. Kumagai, K. Izumiya, H. Takano, Z. Kato, The production of renewable energy in the form of methane using electrolytic hydrogen generation, Energy, Sustainability and Society 4 (17) (2014) 1 – 9. doi:10.1186/s13705-014-0017-5.

[8] M. Thema, F. Bauer, M. Sterner, Power-to-Gas: Electrolysis and methanation status review, Renewable and Sustainable Energy Reviews 112 (2019) 775 – 787. doi:10.1016/j.rser.2019.06.030.

[9] C. Wulf, J. Linßen, P. Zapp, Review of Power-to-Gas Projects in Europe, Energy Procedia 155 (2018) 367 – 378. doi:10.1016/j.egypro.2018.11.041.

[10] J. Gao, Y. Wang, Y. Ping, D. Hu, G. Xu, F. Gu, et al., A thermodynamic analysis of methanation reactions of carbon oxides for the production of synthetic natural gas, RSC Adv. 2 (2012) 2358–2368. doi:10.1039/C2RA00632D.

[11] K. Müller, M. Städter, F. Rachow, D. Hoffmannbeck, D. Schmeißer, Sabatier-based CO_2-methanation by catalytic conversion, Environmental Earth Sciences 70 (2013) 3771–3778. doi:10.1007/s12665-013-2609-3.

[12] O. Buchholz, A. van der Ham, R. Veneman, D. Brilman, S. Kersten, Power-to-Gas: Storing Surplus Electrical Energy. A Design Study, En-

ergy Procedia 63 (2014) 7993 – 8009. doi:10.1016/j.egypro.2014.11.836.

[13] V. Eveloy, Hybridization of solid oxide electrolysis-based power-to-methane with oxyfuel combustion and carbon dioxide utilization for energy storage, Renewable and Sustainable Energy Reviews 108 (2019) 550 – 571. doi:10.1016/j.rser.2019.02.027.

[14] M. Kühn, M. Streibel, N. Nakaten, T. Kempka, Integrated Underground Gas Storage of CO_2 and CH_4 to Decarbonise the "Power-to-gas-to-gas-to-power" Technology, Energy Procedia 59 (2014) 9 – 15. doi:10.1016/j.egypro.2014.10.342.

[15] N. Kezibri, C. Bouallou, Conceptual design and modelling of an industrial scale power to gas-oxy-combustion power plant, International Journal of Hydrogen Energy 42 (30) (2017) 19411 – 19419. doi:10.1016/j.ijhydene.2017.05.133.

[16] M. Bailera, N. Kezibri, L. M. Romeo, S. Espatolero, P. Lisbona, C. Bouallou, Future applications of hydrogen production and CO_2 utilization for energy storage: Hybrid Power to Gas-Oxycombustion power plants, International Journal of Hydrogen Energy 42 (19) (2017) 13625 – 13632. doi:10.1016/j.ijhydene.2017.02.123.

[17] N. Kezibri, Etude dynamique du procédé de production de méthane à partir d'hydrogène électrolytique basse température, PhD, Université Paris Sciences et Lettres (2018).
URL https://pastel.archives-ouvertes.fr/tel-02167350

[18] J. de Bucy, M. Faure, Scenarios and demand for electricity storage

with the EMO concept. Energy and economic assessment of the EMO concept, Report for Fluidstory Project, Enea Consulting (2016).

[19] C. A. Bays, Use of salt cavities for underground storage, in: Symposium on Salt, Northern Ohio Geological Society, Cleveland, Ohio, 1963, pp. 564–578.

[20] R. Thoms, R. Gehle, A brief history of salt cavern use, in: Geertman (Ed.), Proceedings 8th World Salt Symposium, The Hague, 2000, pp. 207–214.

[21] A. Gillhaus, Natural Gas Storage in salt caverns - present status, developments and future trends in Europe, in: Proceedings SMRI Fall Meeting, Basel, 2007.

[22] S. Bachu, M. Dusseault, Underground Injection of Carbon Dioxide in Salt Beds, Developments in Water Science 52 (2005) 637–648. doi:10.1016/S0167-5648(05)52049-5.

[23] J. Shi, S. Durucan, CO_2 storage in caverns and mines, Oil & Gas Science and Technology - Rev. IFP 60 (3) (2005) 569–571.

[24] A. Soubeyran, A. Rouabhi, C. Coquelet, Thermodynamic analysis of carbon dioxide storage in salt caverns to improve the Power-to-Gas process, Applied Energy 242 (2019) 1090 – 1107. doi:10.1016/j.apenergy.2019.03.102.

[25] H. Blanco, A. Faaij, A review at the role of storage in energy systems with a focus on Power to Gas and long-term storage, Renewable and Sustainable Energy Reviews 81 (2018) 1049 – 1086. doi:10.1016/j.rser.2017.07.062.

[26] C. R. Matos, J. F. Carneiro, P. P. Silva, Overview of Large-Scale Underground Energy Storage Technologies for Integration of Renewable Energies and Criteria for Reservoir Identification, Journal of Energy Storage 21 (2019) 241 – 258. doi:10.1016/j.est.2018.11.023.

[27] C. Guo, L. Pan, K. Zhang, C. M. Oldenburg, C. Li, Y. Li, Comparison of compressed air energy storage process in aquifers and caverns based on the Huntorf CAES plant, Applied Energy 181 (2016) 342 – 356. doi:10.1016/j.apenergy.2016.08.105.

[28] D. G. Caglayan, N. Weber, H. U. Heinrichs, J. Linßen, M. Robinius, P. A. Kukla, et al., Technical potential of salt caverns for hydrogen storage in Europe, International Journal of Hydrogen Energy 45 (11) (2020) 6793 – 6805. doi:10.1016/j.ijhydene.2019.12.161.

[29] J. Gernert, R. Span, EOS–CG: A Helmholtz energy mixture model for humid gases and CCS mixtures, The Journal of Chemical Thermodynamics 93 (2016) 274 – 293. doi:10.1016/j.jct.2015.05.015.

[30] S. Heusermann, O. Rolfs, U. Schmidt, Nonlinear finite-element analysis of solution mined storage caverns in rock salt using the LUBBY2 constitutive model, Computers & Structures 81 (8–11) (2003) 629 – 638. doi:10.1016/S0045-7949(02)00415-7.

[31] K. Staudtmeister, R. Rokahr, Rock mechanical design of storage caverns for natural gas in rock salt mass, International Journal of Rock Mechanics and Mining Sciences 34 (3–4) (1997) 300.e1 – 300.e13. doi:10.1016/S1365-1609(97)00199-8.

[32] P. Bérest, The mechanical behavior of salt and salt caverns, in: Eurock

2013, The 2013 ISRM International Symposium, ISRM National Group Poland & Wrocław University of Technology, Wrocław, 2013.

[33] D. Nguyen Minh, S. Brahams, J. Durup, Surface subsidence over deep solution mined storage cavern field, in: 3rd International Conference on Case Histories in Geotechnical Engineering, no. 615, University of Missouri, St. Louis, Missouri, 1993.

[34] H. Djizanne, P. Bérest, B. Brouard, Tensile effective stresses in hydrocarbon storage caverns, in: Proceedings SMRI Fall Meeting, Bremen, 2012.

[35] W. Minkley, M. Knauth, T. Fabig, N. Farag, Stability and integrity of salt caverns under consideration of hydro-mechanical loading, in: Roberts, Mellegard, Hansen (Eds.), Proceedings Saltmech8, Rapid City, SD, 2015, pp. 217–227.

[36] K. Khaledi, E. Mahmoudi, M. Datcheva, T. Schanz, Analysis of compressed air storage caverns in rock salt considering thermo-mechanical cyclic loading, Environmental Earth Sciences 75 (15) (2016). doi:10.1007/s12665-016-5970-1.

[37] P. Labaune, A. Rouabhi, M. Tijani, L. Blanco-Martín, T. You, Dilatancy Criteria for Salt Cavern Design: A Comparison Between Stress- and Strain-Based Approaches, Rock Mechanics and Rock Engineering 51 (2) (2018) 599–611. doi:10.1007/s00603-017-1338-4.

[38] M. Jaschik, M. Tańczyk, A. Janusz-Cygan, A. Wojdyła, K. Warmuziński, The separation of carbon dioxide from $CO_2/N_2/O_2$ mixtures

using polyimide and polysulphone membranes, Chemical and Process Engineering vol. 39 (No 4) (2018) 449–456. doi:10.24425/122962.

[39] U. Setzmann, W. Wagner, A New Equation of State and Tables of Thermodynamic Properties for Methane Covering the Range from the Melting Line to 625 K at Pressures up to 100 MPa, Journal of Physical and Chemical Reference Data 20 (6) (1991) 1061–1155. doi:10.1063/1.555898.

[40] R. Span, W. Wagner, Equations of State for Technical Applications. II. Results for Nonpolar Fluids, International Journal of Thermophysics 24 (2003) 41–109. doi:10.1023/A:1022310214958.

[41] R. Span, W. Wagner, A New Equation of State for Carbon Dioxide Covering the Fluid Region from the Triple-Point Temperature to 1100 K at Pressures up to 800 MPa, Journal of Physical and Chemical Reference Data 25 (6) (1996) 1509–1596. doi:10.1063/1.555991.

[42] P. Bérest, B. Brouard, Safety of Salt Caverns Used for Underground Storage, Oil & Gas Science and Technology - Rev. IFP 58 (3) (2003) 361–384.

[43] P. Bérest, B. Brouard, F. Favret, G. Hévin, M. Karimi-Jafari, Maximum Pressure in Gas Storage Caverns, in: Proceedings SMRI Spring Meeting, Rochester, NY, 2015.

[44] K. Serbin, J. Ślizowski, K. Urbańczyk, S. Nagy, The influence of thermodynamic effects on gas storage cavern convergence, International Journal of Rock Mechanics and Mining Sciences 79 (2015) 166 – 171. doi:10.1016/j.ijrmms.2015.08.017.

[45] R. Wolters, K.-H. Lux, U. Düsterloh, Evaluation of rock salt barriers with respect to tightness: Influence of thermomechanical damage, fluid infiltration and sealing/healing, in: Bérest, Ghoreychi, Hadj-Hassen, Tijani (Eds.), Proceedings Saltmech7, Paris, 2012, pp. 425–434.

[46] Z. Duan, R. Sun, An improved model calculating CO_2 solubility in pure water and aqueous NaCl solutions from 273 to 533 K and from 0 to 2000 bar, Chemical Geology 193 (3) (2003) 257 – 271. doi:10.1016/S0009-2541(02)00263-2.

[47] N. Spycher, K. Pruess, CO_2-H_2O mixtures in the geological sequestration of CO_2. II. Partitioning in chloride brines at 12–100 C and up to 600 bar, Geochimica et Cosmochimica Acta 69 (13) (2005) 3309 – 3320. doi:10.1016/j.gca.2005.01.015.

[48] C. Yaws, J. Hopper, X. Wang, A. Rathinsamy, R. Pike, Calculating solubility & Henry's law constants for gases in water, Chemical Engineering 106 (1999) 102 – 105.

[49] D. Aaron, C. Tsouris, Separation of CO_2 from Flue Gas: A Review, Separation Science and Technology 40 (1-3) (2005) 321–348. doi:10.1081/SS-200042244.

[50] F. Wu, M. D. Argyle, P. A. Dellenback, M. Fan, Progress in O_2 separation for oxy-fuel combustion–A promising way for cost-effective CO_2 capture: A review, Progress in Energy and Combustion Science 67 (2018) 188 – 205. doi:10.1016/j.pecs.2018.01.004.

[51] A. F. Ghoniem, A. Mitsos, Y. Shao-Horn, M. A. Habib, K. Mezghani,

680 R. Ben-Mansour, Integrated polymeric-ceramic membrane based oxy-
681 fuel combustor, US Patent 9004909B2 (2015).

682 [52] G. Wiciak, J. Kotowicz, Experimental stand for CO_2 membrane sepa-
683 ration, Journal of Power Technologies 91 (4) (2011) 171–178.

684 [53] T. C. Merkel, H. Lin, X. Wei, R. Baker, Power plant post-combustion
685 carbon dioxide capture: An opportunity for membranes, Journal of
686 Membrane Science 359 (1) (2010) 126 – 139. doi:10.1016/j.memsci.
687 2009.10.041.

688 [54] L. Zhao, R. Menzer, E. Riensche, L. Blum, D. Stolten, Concepts and
689 investment cost analyses of multi-stage membrane systems used in post-
690 combustion processes, Energy Procedia 1 (1) (2009) 269 – 278. doi:
691 10.1016/j.egypro.2009.01.038.

692 [55] O. Kunz, W. Wagner, The GERG-2008 Wide-Range Equation of State
693 for Natural Gases and Other Mixtures: An Expansion of GERG-2004,
694 Journal of Chemical & Engineering Data 57 (11) (2012) 3032–3091.
695 doi:10.1021/je300655b.

696 [56] S. Ahamada, A. Valtz, S. Chabab, L. Blanco-Martín, C. Coquelet, Ex-
697 perimental Density Data of Three Carbon Dioxide and Oxygen Binary
698 Mixtures at Temperatures from 276 to 416 K and at Pressures up to
699 20MPa, Journal of Chemical & Engineering Data 65 (11) (2020) 5313–
700 5327. doi:10.1021/acs.jced.0c00484.

701 [57] M. Mantovani, P. Chiesa, G. Valenti, M. Gatti, S. Consonni, Supercrit-
702 ical pressure–density–temperature measurements on CO_2–N_2, CO_2–O_2

and CO_2–Ar binary mixtures, The Journal of Supercritical Fluids 61 (2012) 34 – 43. doi:10.1016/j.supflu.2011.09.001.

[58] A. Rouabhi, G. Hévin, A. Soubeyran, P. Labaune, F. Louvet, A multiphase multicomponent modeling approach of underground salt cavern storage, Geomechanics for Energy and the Environment 12 (2017) 21 – 35. doi:10.1016/j.gete.2017.08.002.

[59] L. Blanco Martín, J. Rutqvist, J. T. Birkholzer, Long-term modeling of the thermal–hydraulic–mechanical response of a generic salt repository for heat-generating nuclear waste, Engineering Geology 193 (2015) 198 – 211. doi:10.1016/j.enggeo.2015.04.014.

[60] H. Alkan, Percolation model for dilatancy-induced permeability of the excavation damaged zone in rock salt, International Journal of Rock Mechanics and Mining Sciences 46 (4) (2009) 716–724. doi:10.1016/j.ijrmms.2008.08.002.

[61] P. Bérest, V. de Greef, B. Brouard, Salt Permeability Testing-The Influence of Permeability and Stress on Spherical Hollow Salt Samples, Part II, Research Report RR2001-8-2, SMRI (2003).

[62] P. Cosenza, M. Ghoreychi, B. Bazargan-Sabet, G. de Marsily, In situ rock salt permeability measurement for long term safety assessment of storage, International Journal of Rock Mechanics and Mining Sciences 36 (4) (1999) 509–526. doi:10.1016/S0148-9062(99)00017-0.

[63] U. Hunsche, Determination of the dilatancy boundary and damage up to failure for four types of salt at different stress geometries, in: Fourth

conference on the Mechanical behavior of salt, Trans Tech Publications, 1996, pp. 163–174.

[64] K. Kuhlman, D. Sevougian, Establishing the Technical Basis for Disposal of Heat-Generating Waste in Salt, Report FCRD-UFD-2013-000233, Sandia National Laboratories (2013).

[65] W. Liu, N. Muhammad, J. Chen, C. Spiers, C. Peach, J. Deyi, Y. Li, Investigation on the permeability characteristics of bedded salt rocks and the tightness of natural gas caverns in such formations, Journal of Natural Gas Science and Engineering 35 (2016) 468–482. doi:10.1016/j.jngse.2016.07.072.

[66] J. Stormont, In situ gas permeability measurements to delineate damage in rock salt, International Journal of Rock Mechanics and Mining Sciences 34 (7) (1997) 1055–1064. doi:10.1016/S1365-1609(97)90199-4.

[67] T. Popp, H. Kern, Ultrasonic wave velocities, gas permeability and porosity in natural and granular rock salt, Physics and Chemistry of the Earth 23 (3) (1998) 373 – 378.

[68] H. Sutherland, S. Cave, Argon gas permeability of New Mexico rock salt under hydrostatic compression, International Journal of Rock Mechanics and Mining Sciences & Geomechanics Abstracts 17 (5) (1980) 281–288. doi:10.1016/0148-9062(80)90810-4.

[69] D. Zhang, Experimental investigation of gas transfer properties and stress coupling effects of salt rocks, Ph.D. thesis, Centrale Lille (2021).

[70] P. Bérest, B. Brouard, M. Karimi-Jafari, A. Réveillère, Maximum admissible pressure in salt caverns used for brine production and hydrocarbon storage, Oil & Gas Science and Technology - Rev. IFP 75 (2020). doi:10.2516/ogst/2020068.

[71] P. Bérest, A. Réveillère, D. Evans, M. Stöwer, Review and analysis of historical leakages from storage salt caverns wells, Oil & Gas Science and Technology - Rev. IFP 74 (2019). doi:10.2516/ogst/2018093.

[72] K.-H. Lux, U. Düsterloh, R. Wolters, Long-term behavior of sealed brine-filled cavities in rock salt mass - a new approach for physical modelling and numerical simulation, in: SMRI Fall 2006 conference. Rapid City, SD, 2006.

[73] M. Tijani, G. Vouille, B. Hugout, Le sel gemme en tant que liquide visqueux, in: 5^{th} International Congress on Rock Mechanics, Balkema, Rotterdam, Melbourne, Australia, 1983, pp. 241–246.

[74] Z. Hou, Mechanical and hydraulic behavior of rock salt in the excavation disturbed zone around underground facilities, International Journal of Rock Mechanics and Mining Sciences 40 (5) (2003) 725 – 738. doi:10.1016/S1365-1609(03)00064-9.

[75] K.-H. Lux, Design of salt caverns for the storage of natural gas, crude oil and compressed air: Geomechanical aspects of construction, operation and abandonment, in: D. Evans, R. Chadwick (Eds.), Underground Gas Storage: Worldwide Experiences and Future Development in the UK and Europe, Geological Society London, Special Publications, 2009, pp. 93–128. doi:10.1144/SP313.7.

[76] K. Lux, Gebirgsmechanischer Entwurf und Felderfahrungen im Salzkavernenbau: ein Beitrag zur Entwicklung von Prognosemodellen für den Hohlraumbau im duktilen Salzgebirge, Ferdinand Enke Verlag, Stuttgart, 1984.

[77] O. Schulze, T. Popp, H. Kern, Development of damage and permeability in deforming rock salt, Engineering Geology 61 (2) (2001) 163 – 180. doi:10.1016/S0013-7952(01)00051-5.

[78] S. Donadei, G.-S. Schneider, Chapter 6 - Compressed Air Energy Storage in Underground Formations, in: T. M. Letcher (Ed.), Storing Energy, Elsevier, Oxford, 2016, pp. 113–133. doi:10.1016/B978-0-12-803440-8.00006-3.

[79] Électricité de France (EDF), last accessed February 9, 2021 (2021). [link].
URL https://www.edf.fr/en/meta-home

[80] E. Mahmoudi, K. Khaledi, A. v. Blumenthal, D. König, T. Schanz, Concept for an integral approach to explore the behavior of rock salt caverns under thermo-mechanical cyclic loading in energy storage systems, Environmental Earth Sciences 75 (06 2016). doi:10.1007/s12665-016-5850-8.

- Analysis of CO_2, O_2 and CH_4 storage in salt caverns
- The numerical simulations couple thermodynamics and thermomechanics
- Results suggest salt caverns would be stable and respect common design criteria
- Combined storage of CO_2-O_2 could reduce the number of caverns needed

Credit Author Statement

Laura Blanco-Martín: conceptualization, methodology, analysis, writing
Ahmed Rouabhi: methodology, software, validation
Faouzi Hadj-Hassen: conceptualization, resources, funding acquisition

Declaration of interests

The authors declare that they have no known competing financial interests or personal relationships that could have appeared to influence the work reported in this paper.